PROCEEDINGS OF SCIENCE

CERN-PH-TH/2008-217

Revisiting strong coupling QCD at finite temperature and baryon density

Michael Fromm
Institute for Theoretical Physics, ETH Zurich, CH-8093 Zurich, Switzerland
E-mail: fromm@phys.ethz.ch

Philippe de Forcrand
Institute for Theoretical Physics, ETH Zurich, CH-8093 Zurich, Switzerland
and
CERN, Physics Department, TH Unit, CH-1211 Geneva 23, Switzerland
E-mail: forcrand@phys.ethz.ch

The strong coupling limit ($\beta_{\rm gauge} = 0$) of lattice QCD with staggered fermions enjoys the same non-perturbative properties as continuum QCD, namely confinement and chiral symmetry breaking. In contrast to the situation at weak coupling, the sign problem which appears at finite density can be brought under control for a determination of the full (μ, T) phase diagram by Monte Carlo simulations. Further difficulties with efficiency and ergodicity of the simulations, especially at the strongly first-order, low-T, finite-μ transition, are addressed respectively with a worm algorithm and multicanonical sampling. Our simulations reveal sizeable corrections to the old results of Karsch and Mütter [1]. Comparison with analytic mean-field determinations of the phase diagram shows discrepancies of $\mathcal{O}(10)$ in the location of the QCD critical point.

The XXVI International Symposium on Lattice Field Theory
July 14 - 19, 2008
Williamsburg, Virginia, USA

Speaker.

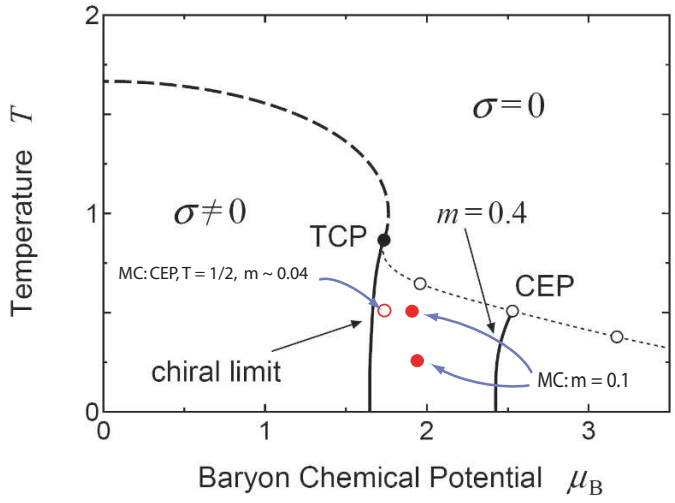

Figure 1: Phase diagram of strong coupling QCD obtained analytically in the mean-field approximation, from [5]. For vanishing quark mass, the first-order transition (solid line) at low temperature turns second-order (dashed line) at a tricritical point (TCP). For non-zero quark mass, the first-order transition ends in a critical endpoint (CEP), whose trajectory as a function of the quark mass is shown by the dotted line. Also displayed are points obtained by the present MC-study: Red dots are transition points for $m = 0.1$, the red circle shows the CEP for $T = 1/2$: ($m \quad 0.038$; $\mu \quad 0.58$).

1. Introduction

We consider lattice QCD with $N_c = 3$ colors and 1 species of staggered fermions (i.e. 4 continuum flavors) at vanishing gauge coupling. The grand canonical partition function is given by

$$Z(m;\mu) = \int \mathcal{D}U\mathcal{D}\bar{\chi}\mathcal{D}\chi\, e^{S_F} \tag{1.1}$$

with

$$S_F = \sum_{x,\nu} \bar{\chi}_x \Big[\eta_{x,\hat{\nu}} U_{x,\hat{\nu}} \chi_{x+\hat{\nu}} \quad \eta_{x,\hat{\nu}}^{-1} U^{\dagger}_{x-\hat{\nu},\hat{\nu}} \chi_{x-\hat{\nu}} \Big] + 2m \sum_x \bar{\chi}_x \chi_x \quad ; \tag{1.2}$$

where $\eta_{x,\hat{\nu}} = e^{\mu}$ $(\nu = 0)$ and $(-1)^{\sum_{\rho<\nu} x_\rho}$ otherwise[1]. Like continuum QCD, this model shows confinement and chiral symmetry breaking. Therefore, it has been the object of numerous analytic studies since the earliest days of lattice QCD, focusing on the mass spectrum [2, 3] and the $(\mu;T)$ phase diagram [4, 5, 6], using increasingly refined treatments, all based on the mean-field approximation. These investigations are continuing to this day [7]. In contrast, very few numerical studies have been performed. Karsch and Mütter [1] showed how to express $Z(m;\mu)$ as a gas of loops, the monomer-dimer-polymer (MDP) ensemble, where the sign problem arising at finite chemical potential is very much reduced. They used this formulation to locate the $T \quad 0$ finite-μ transition, which they found to agree with mean-field predictions. Karsch et al. [8] also found the $\mu = 0$ finite-T transition to be consistent with the expected $O(2)$ universality class in the chiral limit, turning into a crossover for finite quark mass. But a more complete determination of the $(\mu;T)$ phase diagram is lacking. Moreover, Azcoiti et al. [9] reported ergodicity problems with the MDP algorithm

[1] In our notation, all quantities $m;\mu;T;::$ are dimensionless, and should be understood as including the appropriate power of the lattice spacing a.

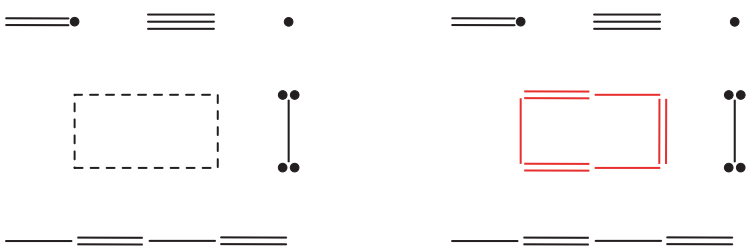

(a) (b)

Figure 2: Sample configuration with (*a*) baryonic loop (dashed line) and (*b*) $D_1 \quad D_2$ polymer loop.

of [1], casting some doubt on the $T \quad 0$, finite μ results. This is particularly interesting because of a mismatch between the critical value of the chemical potential at $T \quad 0$, $\mu_c\,(T \quad 0;m = 0) = 0{:}66$, according to both mean-field [6] and Monte Carlo [1], and the baryon mass $M_B \quad 3$ according to mean-field. One would expect $\mu_c \quad M_B{=}3$, unless the nuclear interaction is strong. A determination of M_B was performed in [10], using conventional HMC at $\beta_{\text{gauge}} = 0$. The value agrees closely with mean-field. Thus, we now want to determine the $(\mu;T)$ phase diagram by Monte Carlo simulations, paying special attention to the value of $\mu_c\,(T \quad 0)$.

The phase diagram can be understood from symmetry considerations. In the chiral limit $m = 0$, the action Eq. (1.2) enjoys the staggered $U(1) \quad U(1)$ symmetry

$$\chi \;!\; e^{i\phi_V + i\varepsilon(x)\phi_A}\chi; \quad \bar{\chi} \;!\; e^{\;i\phi_V + i\varepsilon(x)\phi_A}\bar{\chi}; \quad \varepsilon(x) = \quad 1^{\sum_{\rho=0}^{d} x_\rho} \tag{1.3}$$

where $U(1)_A$ breaks spontaneously at small μ and T, giving rise to a chiral condensate $\sigma \quad \langle\sum_x \bar{\chi}^a_x \chi^a_x\rangle$. Different mean-field approximations all lead to a phase diagram which is qualitatively similar to Fig. 1 with some quantitative differences. The symmetry is restored at large T or μ, by a phase transition which is first-order at low temperature, turning second-order at a tricritical point (TCP), much like what is expected in real QCD with $N_f = 2$ massless flavors. For non-zero quark mass m where $U(1)_A$ is broken explicitly, the second-order transition becomes crossover, and the TCP becomes a critical endpoint (CEP). The behaviour of the CEP as the quark mass is increased is of particular interest, given recent unexpected findings for $N_f = 3$ and $(2+1)$ flavors on coarse lattices [15]. The dotted line in Fig. 1 shows the trajectory of the CEP in the mean-field approximation: it agrees with conventional expectations for real QCD.

2. Theoretical background

The usual strategy to deal with the Grassmann fields $\chi;\bar{\chi}$ in Eq. (1.1) is to integrate them out, which yields the customary fermion determinant. At strong coupling, the absence of a gauge action allows for an alternative strategy: one integrates over the gauge links U first [11]. This leads to (for $N_c = 3$):

$$Z(m;\mu) = \quad \int \mathscr{D}\bar{\chi}\mathscr{D}\chi e^{2m\sum_x \bar{\chi}_x\chi_x} \prod_{x,\nu} F_{x,x+\hat{\nu}} \tag{2.1}$$

with

$$F_{x,x+\hat{\nu}} = \sum_{k=0}^{3} \alpha_k (M_x M_{x+\hat{\nu}})^k + \quad \bar{B}_x B_{x+\hat{\nu}} \eta^3_{x,\hat{\nu}} \quad \bar{B}_{x+\hat{\nu}} B_x \eta^3_{x,\hat{\nu}} \;; \quad \alpha_k = \frac{(N_c \quad k)!}{N_c!k!} : \tag{2.2}$$

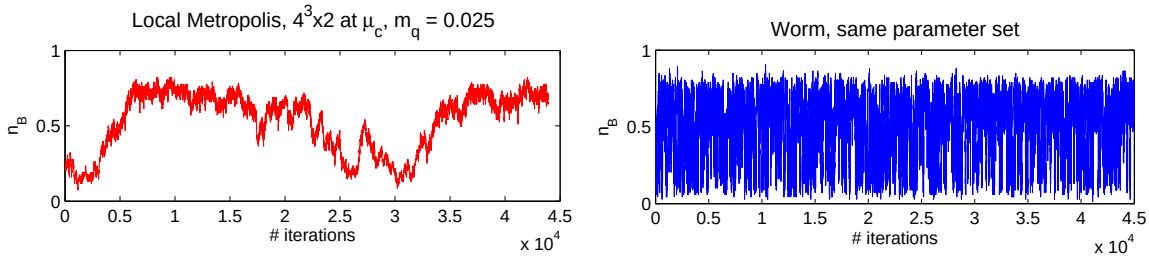

Figure 3: Monte Carlo history of baryon density, for local Metropolis (*left*) and Metropolis+global worm updates (*right*), for runs with $m = 0.025$, $4^3 \quad 2$ at $\mu_c \quad 0.565$ using similar CPU time.

The new degrees of freedom are color singlets: monomers $M_x = \sum_a \bar{\chi}_{ax}\chi_{ax}$, dimers $D_{k,xy} = \frac{1}{k!}(M_xM_y)^k, k = 1,2,3$, and baryons and antibaryons $B_x = \frac{1}{6}\varepsilon_{abc}\chi_{ax}\chi_{bx}\chi_{cx}$, $\bar{B}_x = \frac{1}{6}\varepsilon_{abc}\bar{\chi}_{cx}\bar{\chi}_{bx}\bar{\chi}_{ax}$. Moreover, the Grassmann integration generates a "close-packing" constraint: exactly N_c quarks and N_c antiquarks must be present at each site. This implies that baryon loops C_B, representing $\Pi_{\langle x,y\rangle\in C_B}\bar{B}_xB_y$ in Eq. (2.1), are self-avoiding. It also implies, for the other sites x, that $n_x + \sum_{b_x} n_{b_x} = N_c$, where n_x is the number of monomers on x and n_{b_x} the dimer occupation number (bond number) of the link b_x connected to x (see Fig. 2). Taking this into account we arrive at the final expression

$$Z(m,\mu) = \sum_{\{n_x,n_b,C_B\}} \prod_b \frac{(N_c - n_b)!}{N_c!n_b!} \prod_x \frac{N_c!}{n_x!}(2m)^{n_x} \prod_{C_B} w(C_B) \quad : \tag{2.3}$$

Baryon loops C_B come in two orientations ( ) and carry weight

$$w(C_B, \ ) = \varepsilon(C_B)\exp(\ 3\,\omega L_t\mu), \tag{2.4}$$

where $\varepsilon(C_B)$ is a sign factor depending on the loop geometry, and $\omega \quad 0$ is the winding number around the time direction of extent L_t. There also exist self-avoiding, non-oriented meson loops, which consist of alternating D_1 and D_2 dimers (see Fig. 2(right)). Thus, for a given loop geometry C, the partition function should sum over 4 types of loops: two baryon loops with weights $w(C, \ )$, and two meson loops related by $D_1 \leftrightarrow D_2$, with weight + 1. Karsch and Mütter [1] had the idea of regrouping these 4 contributions in 2 sets, by associating with each meson loop half of $(w(C,+\ ) + w(C, \ ))$. In this way, only non-oriented polymer loops C enter in the partition function, with weight

$$(1 + \varepsilon(C)\cosh(3\,\omega L_t\mu)) \quad : \tag{2.5}$$

The sign problem, which would have been severe in Eq. (2.3), is now much milder. In particular, for $\mu = 0$ one recovers non-negative weights. Moreover, it turns out that the sign problem is very much reduced in comparison with that present in the determinant approach, when one integrates over fermions first. This makes the study of QCD at large μ and low T possible.

3. Algorithmic issues

The MDP system defined by (2.3), (2.5) was sampled in [1] using a local Metropolis algorithm which operates on pairs of neighbouring sites and tries to replace two monomers (one on each

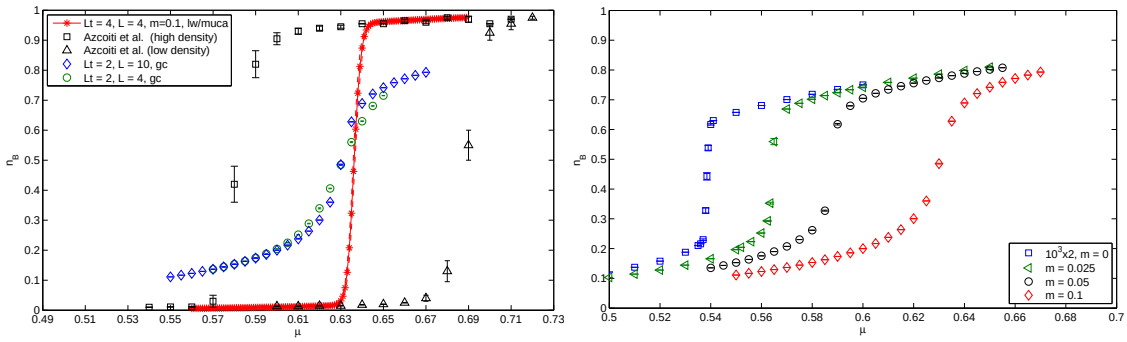

(a) (b)

Figure 4: (*a*) Baryon density n_B versus chemical potential, for systems $L^3 \quad L_t$ at $m = 0:1$, (*b*) same, for masses $m = 0;0:025;0:05;0:1$ and system $10^3 \quad 2$.

site) by a dimer on the connecting link or vice versa. Since a monomer carries weight $\quad m$, this prescription is not ergodic in the chiral limit or the infinite-mass limit. Simulations in [1] were performed over a narrow range of masses. Even so, ergodicity problems were later reported by Azcoiti et al.[9], which cast some doubt on the results of [1]. Therefore we supplement the local Metropolis update above by a worm algorithm [12], which was first adapted to strongly coupled gauge theories in [13]. In Fig. 3 we show the Monte Carlo history of the baryon density in a $4^3 \quad 2$ system at low quark mass m at the critical μ, for both algorithms. The computer time spent is similar in both cases. In the Metropolis case, changing the baryon density proceeds via changing the monomer density, which is very unlikely. In the worm case, a pair of monomers (the head and tail of the worm) is created; then the head is propagated in a succession of nearest-neighbor hops until it meets again the tail and annihilates with it, yielding a new contribution to Z having the same monomer density, but substantially different baryon density. This allows for efficient simulations over the complete range of quark masses. In particular, simulating near or at the chiral limit poses no special problem.

Nevertheless, we still have another difficulty: at low temperature, the finite-μ transition becomes strongly first-order, which makes a correct sampling of the low- and high-density phases problematic. To address this issue, we employ Wang-Landau sampling [14] to extract an estimator for the probability

$$P(O;\mu;m) \quad \sum_{k=\{n_x;n_b;C\}} \delta(O \quad O(k))w_k \tag{3.1}$$

of a suitable observable O such as the energy density $\varepsilon = \frac{1}{V}\frac{\partial}{\partial T}\log Z$ or baryon density $n_B = \frac{1}{3V}\frac{\partial}{\partial \mu}\log Z$. The inverse of the resulting histogram is then used as a weight for multicanonical simulations. Note that the weight w_k defined in Eqs. (2.3) and (2.5) allows for reweighting in both, μ and m, once the numbers of monomers and loops with winding number $'$ for each configuration are known. Hence, the resulting data from multicanonical sampling can be safely reweighted to parameter regions where the corresponding histogram is sufficiently flat.

4. Numerical results

We first reproduced the $\mu = 0;T \quad 0$ results of [10] for the chiral condensate, meson and

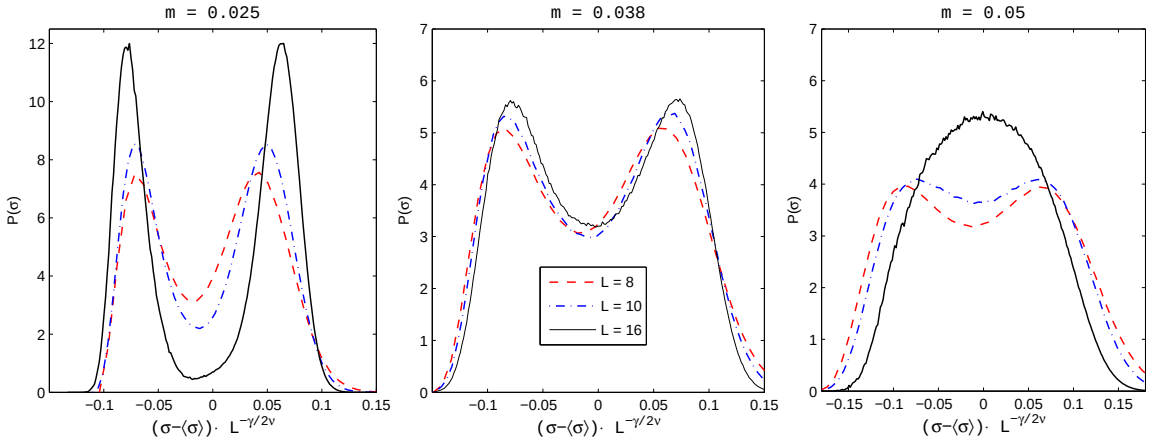

Figure 5: Probability distribution $P(\sigma)$ for masses $m = 0.025, 0.038, 0.05$ tuned to criticality on systems $L^3 \times 2$, $L = 8, 10, 16$. A satisfactory data collapse is observed for the middle mass, using Ising critical exponents.

baryon masses. This is a non-trivial consistency check between the two strategies of first integrating over the gauge links (this work) or the fermions (followed by HMC) [10].

Then, we fix the quark mass to $m = 0.1$ and perform a comparison with [1], who found a phase transition at $\mu \approx 0.69$ on an $8^3 \times 4$ system, i.e. at temperature $T = 1/4$. Fig. 4(a) confirms the problems of ergodicity reported by Azcoiti et al. when using the local Metropolis (data taken from [9]). Already on a 4^4 system, the simulation remains on one of the two metastable branches (density near zero (black triangles) or near the saturation value of 1 baryon per site (black squares)), and one is unable to determine the critical value μ_c of the chemical potential. The Wang-Landau/multicanonical approach allows an ergodic sampling of the critical region. The results (red stars, continuous line) indicate $\mu_c \approx 0.64$, which is significantly smaller than the value ≈ 0.69 of [1], presumably obtained from the end of the metastability branch. Fig. 4(a) also shows higher temperature ($L_t = 2$) results indicating a smoother transition (as expected) and a slight shift of μ_c to smaller values (as opposed to the theoretical predictions of Fig. 1).

We now take full advantage of the worm algorithm and explore the chiral limit at fixed temperature $T = 1/2$ in Fig. 4(b). As the quark mass is reduced, μ_c shifts to smaller values, and the transition becomes first-order, in qualitative agreement with expectations. The order of the transition can only be ascertained by a finite-size scaling study, which is illustrated in Fig. 5. For increasing mass values, the 3 panels each show the probability distribution of the chiral condensate for 3 spatial volumes. In each case, the distribution is reweighted to the pseudo-critical value of μ. The transition is clearly first-order for the smallest mass, and crossover for the largest. For the middle mass, an approximate data collapse is obtained by rescaling the condensate by $L^{\frac{\gamma}{2\nu}}$, using $\gamma = 1.237$ and $\nu = 0.631$ characteristic of the 3d Ising universality class. Indeed, for $m > 0$ the U(1) chiral symmetry is broken explicitly, so we expect no special symmetry breaking other than $Z(2)$ to happen at the transition. Thus, we determine the critical endpoint for temperature $T = 1/2$ to be approximately $(m_c \approx 0.038, \mu_c \approx 0.58)$ (see Fig.1). This can be compared with the mean-field prediction $(m_c \approx 0.4, \mu_c \approx 0.81)$ (Fig. 1) [5]. The discrepancy is an order of magnitude in m_c!

5. Outlook and conclusions

We have presented first results of our study of the strong coupling limit of lattice QCD at finite μ and T. The comparison with mean-field results and with the original Monte Carlo study of Karsch et al. clearly justifies our project. Algorithmic advances largely suppress the ergodicity problems of the latter study, and lead to reliable, new estimates for μ_c over a range of masses. The large discrepancy between exact Monte Carlo and approximate mean-field determinations of the CEP at $T = 1=2$ emphasizes the need for an exact determination of the whole phase diagram. Quantitative mean-field results should be considered with caution.
Our next step includes the determination of the phase diagram in the chiral limit, and the introduction of asymmetric couplings to vary the temperature continuously. As simulations in the chiral limit do not pose any problem for a wide range of parameters, further topics of interest might include a detailed comparison with chiral perturbation theory, and $\rho \; ! \; \pi\pi$ decay.

6. Acknowledgements

The work of M.F. was supported by ETH Research Grant TH-07 07-2.

References

[1] F. Karsch and K. H. Mutter, Nucl. Phys. B **313** (1989) 541.

[2] J. Hoek, N. Kawamoto and J. Smit, Nucl. Phys. B **199** (1982) 495.

[3] H. Kluberg-Stern, A. Morel and B. Petersson, Nucl. Phys. B **215** (1983) 527.

[4] P. H. Damgaard, N. Kawamoto and K. Shigemoto, Nucl. Phys. B **264** (1986) 1.

[5] Y. Nishida, Phys. Rev. D **69** (2004) 094501 [arXiv:hep-ph/0312371].

[6] N. Kawamoto, K. Miura, A. Ohnishi and T. Ohnuma, Phys. Rev. D **75** (2007) 014502 [arXiv:hep-lat/0512023].

[7] K. Miura and A. Ohnishi, arXiv:0806.3357 [nucl-th]; N. Kawamoto, K. Miura and A. Ohnishi, arXiv:0710.1720 [hep-lat]; A. Ohnishi, N. Kawamoto and K. Miura, arXiv:0803.0255 [nucl-th].

[8] G. Boyd, J. Fingberg, F. Karsch, L. Karkkainen and B. Petersson, Nucl. Phys. B **376** (1992) 199.

[9] R. Aloisio et al., Nucl. Phys. B **564** (2000) 489 [arXiv:hep-lat/9910015].

[10] P. de Forcrand and S. Kim, Phys. Lett. B **645** (2007) 339 [arXiv:hep-lat/0608012].

[11] P. Rossi and U. Wolff, Nucl. Phys. B **248** (1984) 105.

[12] N. Prokof'ev and B. Svistunov, Phys. Rev. Lett. **87** (2001) 160601.

[13] D. H. Adams and S. Chandrasekharan, Nucl. Phys. B **662** (2003) 220 [arXiv:hep-lat/0303003].

[14] F. Wang and D. P. Landau, Phys. Rev. Lett. **86** (2001) 2050.

[15] P. de Forcrand and O. Philipsen, JHEP **0701** (2007) 077 [arXiv:hep-lat/0607017]; arXiv:0808.1096 [hep-lat].